Journal of ELECTRONIC MATERIALS, Vol. 38, No. 8, 2009
DOI: 10.1007/s11664-009-0813-4



# Multifunctional ZnO-Based Thin-Film Bulk Acoustic Resonator for Biosensors

YING CHEN,[1] PAVEL I. REYES,[1] ZIQING DUAN,[1] GAURAV SARAF,[1] RICHARD WITTSTRUCK,[1] YICHENG LU,[1,3] OLENA TARATULA,[2] and ELENA GALOPPINI[2]

1.—Department of Electrical and Computer Engineering, Rutgers University, Piscataway, NJ 08854, USA. 2.—Department of Chemistry, Rutgers University, Newark, NJ 07102, USA. 3.—e-mail: ylu@rci.rutgers.edu

Zinc oxide (ZnO) and its ternary alloy magnesium zinc oxide ($Mg_xZn_{1-x}O$) are piezoelectric materials that can be used for high-quality-factor bulk acoustic wave (BAW) resonators operating at GHz frequencies. Thin-film bulk acoustic resonators (TFBARs) are attractive for applications in advanced communication and in various sensors as they offer the capability of monolithic integration of BAW resonators with radio-frequency integrated circuits (RF ICs). In this paper we report $Mg_xZn_{1-x}O$-based TFBAR biosensors. The devices are built on Si substrates with an acoustic mirror consisting of alternating quarter-wavelength silicon dioxide ($SiO_2$) and tungsten (W) layers to isolate the TFBAR from the Si substrate. High-quality ZnO and $Mg_xZn_{1-x}O$ thin films are achieved through a radio-frequency (RF) sputtering technique. Tuning of the device operating frequency is realized by varying the Mg composition in the piezoelectric $Mg_xZn_{1-x}O$ layer. Simulation results based on a transmission-line model of the TFBAR show close agreement with the experimental results. ZnO nanostructures are grown on the TFBAR's top surface using metal-organic chemical vapor deposition (MOCVD) to form the nano-TFBAR sensor, which offers giant sensing area, faster response, and higher sensitivity over the planar sensor configuration. Mass sensitivity higher than $10^3$ Hz cm$^2$/ng is achieved. In order to study the feasibility of the nano-TFBAR for biosensing, the nanostructured ZnO surfaces were functionalized to selectively immobilize DNA, as verified by hybridization with its fluorescence-tagged DNA complement.

**Key words:** Thin-film resonators, biosensors, MgZnO, piezoelectricity, DNA immobilization, nanostructures

## INTRODUCTION

Bulk acoustic wave (BAW) resonators, which are often associated with communication system applications,[1–6] have many advantages, such as small size, low insertion loss, and lower power consumption. Thin-film bulk acoustic wave resonators (TFBARs) are particularly attractive as they offer the capability of monolithic integration of BAW resonators with Si-based radio-frequency integrated circuits (RF ICs), leading to miniaturization by reducing the circuit footprint. Piezoelectric ZnO thin-film transducers are used in a variety of microwave acoustic device applications for the generation and detection of surface acoustic wave (SAW) and BAW due to their high electromechanical coupling coefficients. Various RF devices utilizing piezoelectric ZnO-based TFBARs have been reported, ranging from high-frequency filters to compact, low-power Global System for Mobile Communication (GSM) receivers.[3–6] In addition to

(Received November 22, 2008; accepted April 6, 2009; published online April 25, 2009)

their applications for communications, BAW devices have also been used for sensor applications, such as temperature, pressure, and ambient gaseous atmosphere detection.[7,8] Since TFBARs allow the implementation of BAW devices from several hundred megahertz up to 20 GHz, a higher sensitivity manifested in a large frequency shift per unit mass loading is expected. In addition, TFBAR sensors are much smaller, and can be readily integrated into arrays. Solidly mounted TFBAR sensors can be fabricated on silicon, glass or other substrates using planar technology. The sensors can be integrated with other Si-based electronic components on the same Si substrate. Another distinct advantage of BAW sensors is that they can be used for wireless distance probing in ecological applications. Gabl et al. reported solidly mounted ZnO FBARs with a frequency around 2 GHz for bio- and gas detection with an optimized sensitivity of 2500 Hz $cm^2$/ng, which was 2500 times larger than that of typical 20-MHz quartz crystal microbalance (QCM) sensors.[9] Mai et al. demonstrated ZnO-based FBAR devices for an ultra-mass-sensitive ($0.057 \times 10^5$ Hz $cm^2$/ng) sensor application.[10] An implantable resonant mass sensor was reported for liquid sensing.[11] This sensor has a low $Q$ value (40) at 2 GHz and a 5 ppm resonant frequency shift was detected, corresponding to $10^{-8}$ g/$cm^2$ mass change on the sensor surface.

The recent progress in nanoscale science and technology is promising for the development of novel nanobiosensors with faster response and higher sensitivity and selectivity than those of the planar sensor configurations (due to their nanoscale dimensions), dramatically increased sensing surface area, and strong binding with biological and chemical reagents. Such novel nanostructured sensors can be used to detect gas absorption and biological molecules interactions of DNA–DNA, DNA–RNA, protein–protein, and protein–small molecules. ZnO nanostructures are becoming one of the most promising multifunctional nanostructures, and have found broad applications in optoelectronics, electronics, catalysts, and especially high-sensitivity sensor technology. A nano-SAW sensor, consisting of ZnO nanotips grown on a 128° Y-cut $LiNbO_3$ SAW delay line, greatly enhanced DNA immobilization.[12] ZnO nanorod and nanowire film-coated QCMs were investigated as humidity sensors.[13,14] Surface functionalization of ZnO nanostructures in gas or liquid phase has been studied for biochemical sensing.[15] A ZnO nanotip-based QCM sensor was demonstrated to have a 10-fold larger frequency shift than that of regular QCM sensors when measuring the same DNA oligonucleotide solution.[16] Furthermore, through the wettability control, the superhydrophilic surface of a ZnO nanotip layer on such a sensor significantly boosts solution intake, thereby significantly saving liquid DNA samples and enhancing sensitivity.[17]

A new piezoelectric material, $Mg_xZn_{1-x}O$, which is a ternary alloy of ZnO and MgO, has been discovered and successfully grown.[18,19] ZnO belongs to the wurtzite crystal class, and is a well-known piezoelectric material. In contrast, MgO is a nonpiezoelectric material with a rock-salt cubic structure. For the range of Mg content below approximately 33%, the $Mg_xZn_{1-x}O$ crystal retains the wurtzite structure. In comparison with ZnO, MgO has higher longitudinal and transverse bulk acoustic wave velocities. Thus, $Mg_xZn_{1-x}O$'s acoustic velocity increases and piezoelectric coupling decreases with increasing Mg content. By controlling the Mg mole percentage, the TFR frequency response can be tailored. $Mg_xZn_{1-x}O$ thin-film bulk acoustic wave devices have been demonstrated on *r*-plane sapphire substrates.[20]

In this work, $Mg_xZn_{1-x}O$-based single-mode thin-film bulk acoustic wave resonators (TFBARs) are built on Si substrates. In order to achieve the single-mode TFBAR, an acoustic mirror reflector structure is used to prevent the acoustic wave from transmitting into the Si substrate. The piezoelectric properties are tailored by controlling the Mg composition in the $Mg_xZn_{1-x}O$ film. The TFBARs are adapted for mass-sensitive sensors. ZnO nanotips are grown on TFBAR surface using MOCVD to make the ZnO nano-TFBAR with high mass sensitivity. The ZnO nanostructured surfaces are functionalized through selective DNA immobilization and hybridization for biosensing.

## DEVICE STRUCTURE AND MATERIAL GROWTH

A schematic of the TFBAR device structure consisting of Al/$Mg_xZn_{1-x}O$/Au/acoustic mirror/Si is shown in Fig. 1. For the experiments performed in the "Device Modeling and Testing" section of this paper, the device consists of Al and Au as the top and bottom electrode, respectively. Au is chosen as

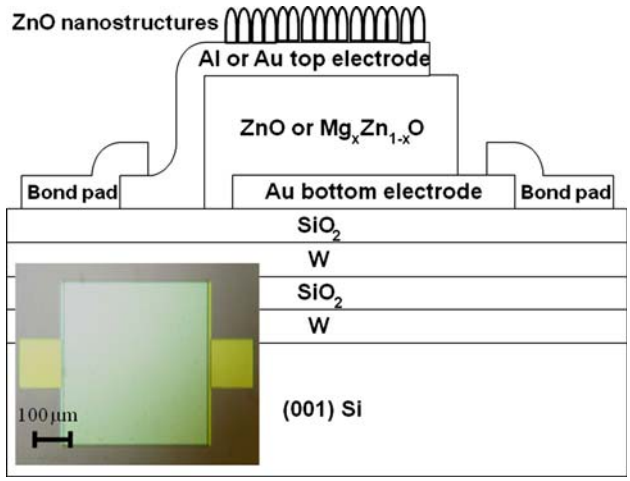


Fig. 1. Schematic diagram of the $Mg_xZn_{1-x}O$/Si TFBAR structure; inset shows an optical microscope image of a TFBAR device. For the TFBAR nanosensor, Au top electrode is used to facilitate MOCVD growth of ZnO nanostructures.

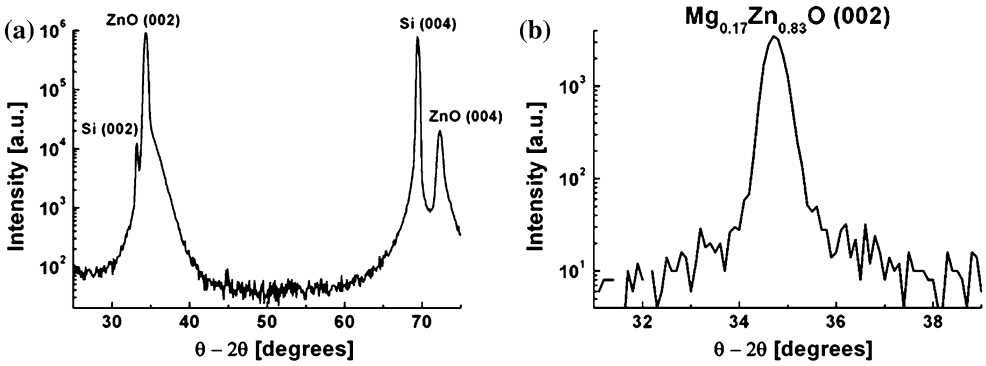


Fig. 2. X-ray $\theta$–$2\theta$ scan of (a) ZnO and (b) $Mg_{0.17}Zn_{0.83}O$ deposited on $SiO_2$/Si.

the bottom electrode to allow deposition of high-quality ZnO and $Mg_xZn_{1-x}O$ thin films on top of it by the RF sputtering technique.[21] Al or Au is used as the top electrode. The Al electrode is used for the regular TFBAR without ZnO nanostructures to minimize the mass loading from the electrode. The acoustic mirror consists of two periods of quarter-wavelength $SiO_2$/W Bragg reflector, which is used to isolate the resonator from the Si substrate. ZnO and $Mg_xZn_{1-x}O$ thin films are used as the piezoelectric layers. When a signal is applied between the top and bottom electrodes, a longitudinal acoustic wave mode is excited. We have also integrated ZnO nanostructures with the TFBAR to form novel biosensors, where the ZnO nanostructures are deposited on a Au top electrode to provide a giant sensing area. The Au top electrode is used instead of Al to facilitate MOCVD growth of ZnO nanostructures with good crystallinity and to avoid oxidation of the metal electrode.

The $c$-axis-oriented ZnO and $Mg_xZn_{1-x}O$ ($0 < x < 0.33$) films were deposited using the RF sputtering technique. As-grown ZnO and $Mg_xZn_{1-x}O$ films generally show $n$-type semiconducting properties due to oxygen vacancies, Zn interstitials, and other defects and impurities. In order to effectively stimulate the piezoelectric effect in ZnO and $Mg_xZn_{1-x}O$, this $n$-type conductivity has to be compensated by heavily doping with species such as Li, Ni or Cu. We made ZnO and $Mg_xZn_{1-x}O$ sputtering targets with Ni doping. The ZnO and $Mg_xZn_{1-x}O$ sputtering targets were prepared by mixing appropriate quantities of 99.99% pure ZnO and MgO powders with 2 wt.% NiO powder for compensation doping. The ZnO and $Mg_xZn_{1-x}O$ films deposited from these targets do not require postdeposition diffusion at high temperature.

The sputtering chamber is equipped with a standard RF power source. Before deposition, the chamber was kept at a vacuum level of $5.0 \times 10^{-6}$ Torr. During deposition, a mixture of 1:1 Ar and $O_2$ was fed into the chamber, with the pressure of the chamber maintained at $7.5 \times 10^{-3}$ Torr. The substrate was heated at 400°C to achieve films with good crystal quality and surface morphology. A ZnO buffer layer (50 nm) was first deposited, followed by deposition of a thicker film at a deposition rate higher than 0.7 $\mu$m/h.

The crystallographic orientation and structural quality of the as-grown films were determined using a Bruker D8 Discover four-circle x-ray diffractometer (XRD). Figure 2a shows an x-ray $\theta$–$2\theta$ scan of ZnO and $Mg_{0.17}Zn_{0.83}O$ sputtered on $SiO_2$/Si. The scan is done using $CuK_\alpha$ radiation to analyze the orientation of the ZnO film. A ZnO (002) peak is observed at ~34.3°, indicating a predominantly $c$-axis-oriented ZnO film. Figure 2b shows the x-ray $\theta$–$2\theta$ scan of predominantly $c$-axis-oriented $Mg_{0.17}Zn_{0.83}O$ (002) with a peak at ~34.7°.

The surface morphology of the $Mg_xZn_{1-x}O$ films was characterized using a Leo-Zeiss field-emission scanning electron microscope (FESEM). Figure 3a shows an FESEM image of a $Mg_{0.2}Zn_{0.8}O$ thin film deposited on the mirror/Si structure. The image is taken from the active region of the device where the film is directly on the acoustic mirror, rather than on the Au bottom electrode. The $Mg_{0.2}Zn_{0.8}O$ film has a dense columnar structure, with smooth surface. The two-period acoustic mirror structure (750 nm $SiO_2$ and 720 nm W) is clearly visible as alternating light and dark layers.

Single-crystalline ZnO nanostructures of 200 nm height and 70 nm diameter were directly grown on a Au electrode by MOCVD. The details of the MOCVD growth have been reported earlier.[22,23] Diethyl zinc (DEZn) and $O_2$ are used as the Zn source and oxidizer, respectively. The substrate temperature was maintained at ~475°C and the chamber pressure at ~50 Torr during the MOCVD growth. An FESEM image of the vertically aligned ZnO nanostructures is shown in Fig. 3b.

## DEVICE MODELING AND TESTING

### Tuning of Resonant Frequency Using $Mg_xZn_{1-x}O$

The three-port transmission-line model[24] was used to analyze behavior of the acoustic waves propagating in the $Mg_xZn_{1-x}O$ thin-film resonators built on Si substrates, as shown in Fig. 4.

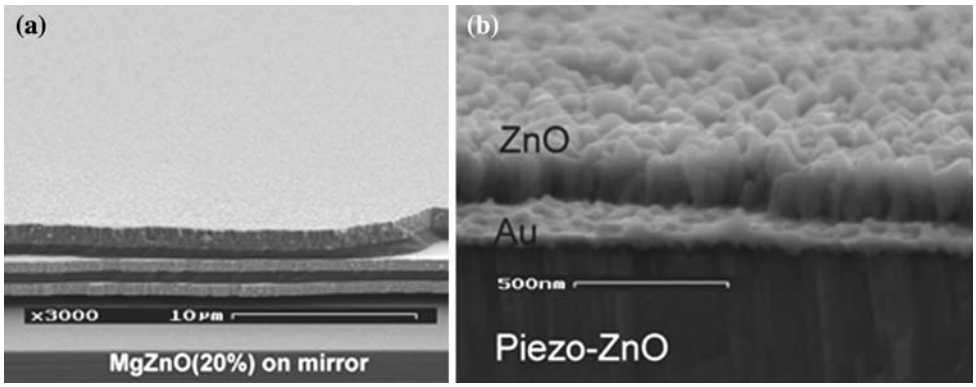


Fig. 3. Cross-sectional FESEM images of (a) $Mg_{0.2}Zn_{0.8}O$ film deposited on the mirror/Si structure and (b) ZnO nanostructures deposited on Au electrodes.

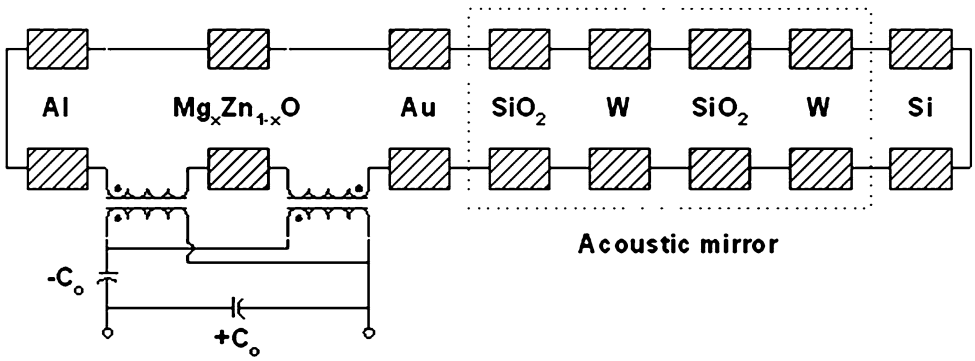


Fig. 4. Transmission-line model for the multilayer TFBAR structure used for simulation of the frequency response of the device.

The resonator only excites the longitudinal wave mode, hence the circuit model only consists of the piezoelectrically active longitudinal branch.

This equivalent circuit model of the multilayer structure of the TFBAR was constructed using a modular building-block approach, wherein each layer corresponds to a network feature. The acoustic impedances of W and $SiO_2$ are $97.40 \times 10^6$ kg s$^{-1}$ m$^{-2}$ and $13.25 \times 10^6$ kg s$^{-1}$ m$^{-2}$, respectively. The reflectivity of the W-$SiO_2$ interface is:

$$R_{W,SiO_2} = \frac{Z_W - Z_{SiO_2}}{Z_W + Z_{SiO_2}} \approx 0.79. \quad (1)$$

The two-period mirror structure effectively isolates the main resonance. In order to completely eliminate the spurious resonances from the substrate, a multiple-period mirror structure should be used.

RF characterization of the TFBAR devices was conducted using an HP 8573D network analyzer (Agilent Technologies, Palo Alto, CA) and a Cascade Microtech probe station (Cascade Microtech Inc., Beaverton, OR). The reflection parameter $S_{11}$ of the thin-film resonator was measured and the longitudinal acoustic velocity was calculated. The operating frequency of the TFBAR was measured for the corresponding mole fraction of Mg in the $Mg_xZn_{1-x}O$ film. Figure 5 shows the $S_{11}$ spectra of $Mg_xZn_{1-x}O$ TFBARs whose device area is 400 $\mu$m $\times$ 400 $\mu$m. The solid line is the frequency response of a TFBAR with a 1.12-$\mu$m-thick ZnO layer; the resonance frequency is at 2.04875 GHz with $S_{11} = -13.14$ dB.

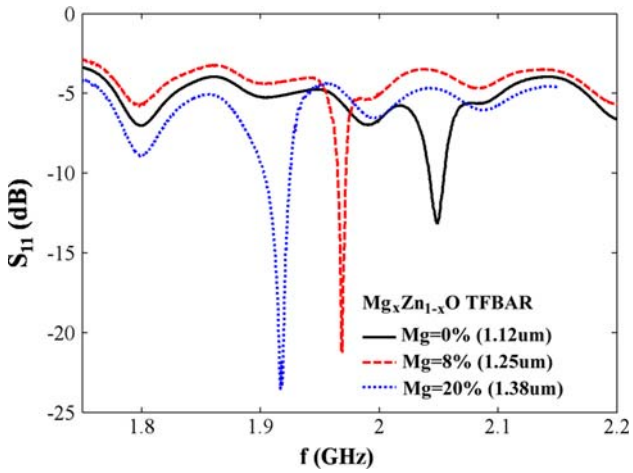


Fig. 5. Measured $S_{11}$ spectra of the $Mg_xZn_{1-x}O$ TFBARs with varying Mg compositions $x = 0$, 0.17, and 0.20 in the $Mg_xZn_{1-x}O$ films. The experimental results closely match the simulation results.

The dashed line represents a TFBAR with a 1.25-$\mu$m-thick $Mg_{0.08}Zn_{0.92}O$ layer; the resonance frequency is at 1.96875 GHz with $S_{11} = -21.19$ dB. The dotted line presents a $Mg_{0.2}Zn_{0.8}O$ TFBAR with film thickness of about 1.38 $\mu$m; the resonance frequency is at $f = 1.91687$ GHz and $S_{11} = -23.5$ dB. The simulation results based on the transmission-line model reveal that the resonant frequency of the thin-film resonator can be tailored by using different mole fractions of Mg in the piezoelectric $Mg_xZn_{1-x}O$ layer. The series resonant frequency $f$ is determined by the ratio of the phase velocity, $v$, and the thickness of the piezoelectric layer, $h$:

$$f = \frac{v}{2h}. \tag{2}$$

The calculated phase velocity increases 7% when the Mg mole composition increases from 0% to 2%. The measured data of the resonant frequency corresponding to various mole fractions of Mg in $Mg_xZn_{1-x}O$ agree closely with the simulation results. The calculated phase velocities from $S_{11}$ measurements are 4,589 m/s for ZnO, 4,922 m/s for $Mg_{0.08}Zn_{0.92}O$, and 5,291 m/s for $Mg_{0.2}Zn_{0.8}O$.

### Device Calibration and Mass Loading Sensitivity

The sensitivity due to the mass loading effect is calculated using Sauerbrey's formula[25]:

$$\Delta f = -\frac{2f_0^2}{A\sqrt{c_{66}\rho}}\Delta m = -S_f \Delta m, \tag{3}$$

where $f_0$ is the reference resonant frequency and $f_0 + \Delta f$ is the loaded frequency, $c_{66}$ is the stiffness constant of the piezoelectric material, and $\rho$ is the density of the piezoelectric material. In the case of ZnO, $c_{66} = 4.43 \times 10^{10}$ N/m$^2$ and $\rho = 5680$ kg/m$^3$. The TFBAR used for sensitivity measurement has a piezoelectric ZnO layer with a thickness of 1.24 $\mu$m. To determine the mass loading sensitivity $S_f$, we deposited a 60-nm layer of $SiO_2$ on the top electrode (with area of 150 $\mu$m $\times$ 150 $\mu$m) of the TFBAR using plasma-enhanced chemical vapor deposition (PECVD). The density of $SiO_2$ deposited by PECVD is 2.3 g/cm$^3$. The measured frequency shift due to the deposited $SiO_2$ layer is 23.7 MHz, as shown in Fig. 6. The experimental mass sensitivity $S_f$ of $1.72 \times 10^3$ Hz cm$^2$/ng is achieved, which is useful for ultrasensitive mass loading sensor applications.

## FUNCTIONALIZATION OF ZnO NANOSTRUCTURES FOR BIOSENSING

ZnO nanostructures were integrated with the TFBAR to form the ZnO nano-TFBAR. The ZnO nanostructures were grown directly on the top electrode by MOCVD as described in the "Device Structure and Material Growth" section. The ZnO nanostructures have the advantage of controllable wettability, which allows it to be a superhydrophilic surface. The superhydrophilic property of the nanostructured TFBAR surfaces allows for the consumption of much less liquid samples during sensing.

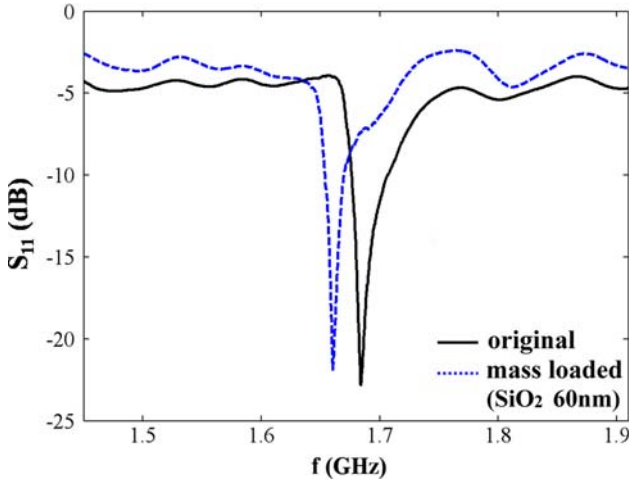


Fig. 6. Measured $S_{11}$ spectra of a 150 $\mu$m $\times$ 150 $\mu$m ZnO TFR built on a mirror/Si substrate, before and after deposition of 60 nm $SiO_2$ as mass loading. Frequency shift due to mass loading results in 1.72 kHz/ng sensitivity.

The functionalization of the nanostructured ZnO sensing surface enables the nanostructures to selectively bind only to the prescribed set of biomolecules. The functionalization scheme was used to implement the selective binding of specific DNA oligonucleotides onto the nanostructured ZnO surface, which were then hybridized with their fluorescent-tagged complements. An optimized chemical functionalization scheme was developed for the ZnO nanostructures on the nano-TFBAR. The detailed chemical binding analysis will be published elsewhere.[26] A set of optimized linkers to functionalize ZnO with DNA in this work can be summarized in three steps (as shown in Fig. 7): step 1: ZnO + linker, step 2: DNA immobilization, and step 3: fluorescence-tagged DNA hybridization. After every

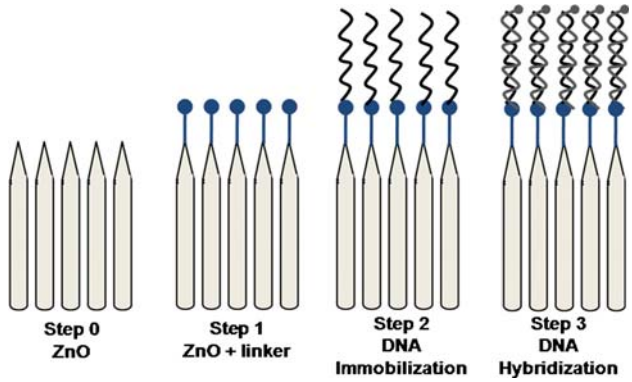


Fig. 7. Simplified schematic of the chemical functionalization process for the ZnO nanotips to implement selective DNA immobilization and hybridization.

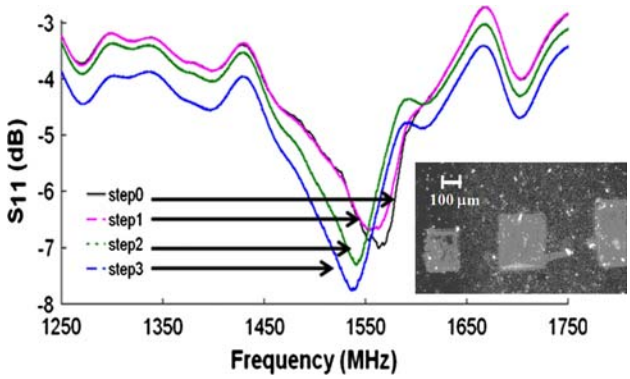


Fig. 8. Frequency shift due to mass loading on the nano-TFBAR, step 0: nano-TFBAR only, step 1: adding bifunctional linker, step 2: DNA immobilization, and step 3: DNA hybridization. The inset shows the fluorescence image of three nano-TFBAR sensors on the same substrate where the gray squares correspond to the sensing areas of the nano-TFBAR devices containing the fluorescing hybridized DNA.

step, the nanotips were rinsed with a pH-controlled buffer solution and the $S_{11}$ spectrum of the nano-TFBAR was measured for frequency shift due to mass loading.

Figure 8 shows the frequency shifts of the nano-TFBAR after each chemical step in the optimized functionalization scheme outlined above. The nano-TFBAR sensing area is 0.25 mm × 0.25 mm. The solid black line represents the frequency response of TFBAR before step 1. The frequency peak at minimum insertion loss is 1562.81 MHz. After step 1, the frequency at minimum insertion loss shifted to 1553.75 MHz. After step 2, the frequency at minimum insertion loss shifted further down to 1540.94 MHz. After step 3, the frequency at minimum insertion loss shifted further to 1535.94 MHz. The measured results show that the resonance frequency decreases with increasing mass loaded on the top electrode of the nano-TFBAR. The total frequency shift was about 26 MHz, corresponding to 16.25 ng of hybridized DNA and linker molecules combined. To verify that the immobilized and hybridized DNA molecules only selectively attached to the ZnO nanostructured sensing area, we performed fluorescence measurements on the nano-TFBAR sensing area. The fluorescence image of the nano-TFBAR in the inset of Fig. 8 shows that only the ZnO nanostructured sensing electrode area (bright gray squares) is positively fluorescing. This confirms that the DNA molecules only attached themselves to the ZnO nanostructured sensing area of the nano-TFBAR device. These results demonstrate that the ZnO nano-TFBAR is a promising device for biosensing applications.

## CONCLUSIONS

Thin-film bulk acoustic resonators using the new piezoelectric material $Mg_xZn_{1-x}O$ were demonstrated. The TFBAR devices were built on Si substrates with an acoustic mirror consisting of alternating quarter-wavelength $SiO_2$ and W layers. The mirror isolates the acoustic wave from transmitting into the Si substrate, assuring single-mode operation. The *c*-axis-oriented piezoelectric $Mg_xZn_{1-x}O$ thin films were deposited using RF sputtering on the mirror/Si substrate. The bulk acoustic wave velocity can be tailored by changing the Mg composition in the $Mg_xZn_{1-x}O$. This allows flexibility in TFBAR device design because the resonant frequency can be determined by both thickness and the Mg composition of the piezoelectric film. The mass sensitivity of ZnO-based 1.67-GHz TFBAR is $1.72 \times 10^3$ Hz cm$^2$/ng, which is three orders of magnitude higher than that of a standard QCM. A nano-TFBAR biosensor was made by integrating ZnO nanostructure on the ZnO-based TFBAR device. Selective DNA immobilization and hybridization were realized by optimized functionalization of the nanostructured sensing area.

## ACKNOWLEDGEMENTS

This work has been supported by the NSF (ECS-0224166), New Jersey Commission on Science and Technology (NJCST) with the Research Excellence Center Grant, and AFOSR's DCT Grant.

## REFERENCES

1. K.M. Lakin, G.R. Kline, and K.T. McCarron, *IEEE Ultrasonics Symp.* (1992), p. 471.
2. R. Ruby, P. Bradley, Y. Oshmyansky, A. Chien, and J.D. Larson III, *IEEE Ultrasonics Symp.* (2001), p. 813.
3. L. Mang and F. Hickernell, *Proc. IEEE Int. Freq. Control Symp.* (1996), p. 363.
4. C.W. Seabury, P.H. Kobrin, R. Addison, and D.P. Havens, *IEEE MTT-S Digest* (1997), p. 181.
5. J. Kaitila, M. Ylilammi, J. Molarius, J. Ella, and T. Makkonen, *Proc. IEEE Int. Ultrasonics Symp.* (2001), p. 803.
6. Y.S. Park, S. Pinkett, J.S.Kenney, and W.D. Hunt, *Proc. IEEE Int. Ultrasonics Symp.* (2001), p. 839.
7. P. Hauptmann, R. Lucklum, and J. Schröder, *Proc. IEEE Int. Ultrasonics Symp.* (2003), p. 56.
8. G.D. Mansfeld and I.M. Kotelyansky, *Proc. IEEE Int. Ultrasonics Symp.* (2002), p. 909.
9. R. Gabl, E. Green, M. Schreiter, H.D. Feucht, H. Zeininger, R. Primig, D. Pitzer, G. Eckstein, W. Wersing, W. Reichl, and J. Runck, *Proc. IEEE Sensors*, Vol. 2 (2003), p. 1184.
10. L. Mai, D.H. Kim, M. Yim, and G. Yoon, *Microw. Opt. Technol. Lett.* 42, 505 (2004). doi:10.1002/mop.20351.
11. H. Zhang, M.S. Marma, E.S. Kim, C.E. McKenna, and M.E. Thompson, *17th IEEE Int. Conf. on Micro Electro Mech. Sys.* (2004), p. 347.
12. Z. Zhang, N.W. Emanetoglu, G. Saraf, Y. Chen, P. Wu, J. Zhong, Y. Lu, J. Chen, O. Mirochnitchenko, and M. Inouye, *IEEE Trans. Ultrason. Ferroelectr. Freq. Control* 53, 786 (2006). doi:10.1109/TUFFC.2006.1665081.
13. Y. Zhang, K. Yu, S. Quyang, L. Luo, H. Hu, Q. Zhang, and Z. Zhu, *Physica B* 368, 94 (2005). doi:10.1016/j.physb.2005.07.001.
14. X. Zhou, J. Zhang, T. Jiang, X. Wang, and Z. Zhu, *Sens. Actuators A* 135, 209 (2007). doi:10.1016/j.sna.2006.07.001.
15. O. Taratula, E. Galoppini, D. Wang, D. Chu, Z. Zhang, H. Chen, G. Saraf, and Y. Lu, *J. Phys. Chem. B* 110, 6506 (2006). doi:10.1021/jp0570317.
16. Z. Zhang, H. Chen, J. Zhong, Y. Chen, and Y. Lu, *Proc. IEEE Int. Freq. Contr. Symp.* (2006), p. 545.
17. Z. Zhang, H. Chen, J. Zhong, and Y. Lu, *J. Electron. Mater.* 36, 895 (2007). doi:10.1007/s11664-007-0126-4.

18. N.W. Emanetoglu, S. Muthukumar, P. Wu, R. Wittstruck, and Y. Lu, *IEEE Intl. Ultrason. Symp. Proc.* (2001), p. 253.
19. N.W. Emanetoglu, S. Muthukumar, P. Wu, R. Wittstruck, Y. Chen, and Y. Lu, *IEEE Trans. Ultrason. Ferroelectr. Freq. Control* 50, 537 (2003). doi:10.1109/TUFFC.2003.1201466.
20. R.H. Wittstruck, X. Tong, N.W. Emanetoglu, P. Wu, Y. Chen, J. Zhu, S. Muthukumar, Y. Lu, and A. Ballato, *IEEE Trans. Ultrason. Ferroelectr. Freq. Control* 50, 1272 (2003). doi:10.1109/TUFFC.2003.1244743.
21. Y. Yoshino, K. Inoue, M. Takeuchi, and K. Ohwada, *Vacuum* 5, 601 (1998). doi:10.1016/S0042-207X(98)00257-7.
22. H. Chen, J. Zhong, G. Saraf, Z. Zhang, Y. Lu, L.A. Fetter, and C.S. Pai, *Proc. SPIE* 5592, 164 (2004). doi:10.1117/12.571509.
23. J. Zhong, G. Saraf, S. Muthukumar, H. Chen, Y. Chen, and Y. Lu, *J. Electron. Mater.* 33, 654 (2004). doi:10.1007/s11664-004-0062-5.
24. A. Ballato, Transmission-line Analogs for Piezoelectric Layered Structures (Ph.D. dissertation, Polytechnic Institute of Brooklyn, NY, June 1972).
25. G. Sauerbrey, *Z. Phys.* 155, 206 (1959). doi:10.1007/BF01337937, in German.
26. O. Taratula, R. Mendelsohn, E. Galoppini, P.I. Reyes, Z. Zhang, Y. Chen, G. Saraf, and Y. Lu, *Langmuir* (2009), to appear.